Brownian parametric oscillators

Christine Zerbe, Peter Jung,* and Peter Hänggi
Institute of Physics, University of Augsburg, Memminger Strasse 6, D-86135 Augsburg, Germany
(Received 6 December 1993)

We discuss the stochastic dynamics of dissipative, white-noise-driven Floquet oscillators, characterized by a time-periodic stiffness. Thus far, little attention has been paid to these exactly solvable nonstationary systems, although they carry a rich potential for several experimental applications. Here, we calculate and discuss the mean values and variances, as well as the correlation functions and the Floquet spectrum. As one main result, we find for certain parameter values that the fluctuations of the position coordinate are suppressed as compared to the equilibrium value of a harmonic oscillator (parametric squeezing).

PACS number(s): 05.40.+j

I. INTRODUCTION

Parametric phenomena are ubiquitous in physics. An early example is Faraday's experiment in 1831 when he excited—via vertical vibrations—surface waves in water-filled columns. Other familiar parametric systems are, e.g., electric circuits with a periodic capacitance, or pendulums with a moving support. One of the more modern parametric systems occurring in physics is the quadrupole ion trap, also termed the *Paul trap* [1]. This system is also interesting with regard to quantum-mechanical applications [2]. In nonlinear systems, parametric perturbations are discussed in the context of suppression of chaos [3]. All these systems have in common that they can be described in terms of equations containing parameters which vary periodically in time. The simplest example of such an equation is the Mathieu equation [4]. Up to the present day most of the applications involving the Mathieu equation have been of a deterministic nature. The objective of this work is the study of the Brownian motion of the damped Mathieu equation driven by additive white Gaussian noise. A treatment of this nonstationary stochastic process must be ranked in view of difficulty right after the additively driven Ornstein-Uhlenbeck process [5]; although complex, this system can—due to its inherent linear structure—still be solved *exactly*. However, not much prior stochastic work exists on this Brownian parametric oscillator. In the absence of friction, the covariance matrix has been studied by Gitterman, Shrager, and Weiss [6]. Work by Mazo [7] on the damped parametric oscillator focused on a formal discussion of the covariance matrix in terms of the corresponding time-inhomogeneous Green's function. Very recently interesting experiments on a microparticle in a Paul trap have been performed by Arnold, Folan, and Korn [8]: They detected a distinct minimum in the behavior of the coordinate variance (see below). Their surprising findings motivated the present analytical work wherein we investigate in detail the dynamics of the Brownian parametric oscillator.

The paper is organized as follows. In Sec. II, we present our model together with some background knowledge of nonstationary Fokker-Planck processes. In Sec. III, we discuss the mean values and the covariance matrix. The Floquet spectrum of the corresponding Fokker-Planck operator is studied analytically in Sec. IV. Section V addresses the evaluation of the position autocorrelation function.

II. MODEL AND BASIC EQUATIONS

The Langevin equation for a Brownian particle in a harmonic potential with time-dependent frequency $U(x,t;\varphi)=\frac{1}{2}[\omega_0^2+\epsilon\cos(\Omega t+\varphi)]x^2$ reads

$$\ddot{x}+\gamma\dot{x}+[\omega_0^2+\epsilon\cos(\Omega t+\varphi)]x=\sqrt{\gamma D}\,\xi(t)\ . \tag{1}$$

The parametric modulation is characterized by the amplitude ϵ, the frequency Ω, and an initial phase φ. We assume that the phase is not known, i.e., it is equally distributed between 0 and 2π. The perturbation $\xi(t)$ denotes Gaussian white noise with zero mean and correlation

$$\langle\xi(t)\xi(t')\rangle=2\delta(t-t')\ . \tag{2}$$

When $\epsilon=0$, Eq. (1) reduces to the standard problem of a damped harmonic oscillator driven by Gaussian white noise [9]. The introduction of the scaled variables $\bar{t}=\Omega t/2$, $\bar{\omega}_0^2=4\omega_0^2/\Omega^2$, $\bar{\epsilon}=2\epsilon/\Omega^2$, $\bar{\gamma}=2\gamma/\Omega$, and $\bar{D}=4D/\Omega^2$ yields the normalized equation of motion, i.e.,

$$\ddot{x}+\bar{\gamma}\dot{x}+[\bar{\omega}_0^2+2\bar{\epsilon}\cos(2\bar{t}+\varphi)]x=\sqrt{\bar{\gamma}\bar{D}}\,\xi(\bar{t})\ . \tag{3}$$

From here on we shall exclusively use the normalized form (3), and shall drop the overbars for the sake of convenience.

The rate of change of the probability $P(x,v,t;\varphi)$ corresponding to the nonstationary process in (3) is given by the Fokker-Planck equation

*Present address: University of Illinois at Urbana-Champaign, Beckman Institute, 405 North Mathews Avenue, Urbana, IL 61801.

$$\frac{\partial}{\partial t}P(x,v,t;\varphi)=\mathcal{L}_{\rm FP}(t)P(x,v,t;\varphi)\ , \tag{4a}$$

with

$$\mathcal{L}_{\rm FP}(t)=-\frac{\partial}{\partial x}v+\gamma\frac{\partial}{\partial v}v+\omega_0^2\frac{\partial}{\partial v}x+\gamma D\frac{\partial^2}{\partial v^2}$$
$$+2\epsilon\cos(2t+\varphi)\frac{\partial}{\partial v}x\ . \tag{4b}$$

The periodicity of the Fokker-Planck operator $\mathcal{L}_{\rm FP}$, i.e., $\mathcal{L}_{\rm FP}(t+\pi)=\mathcal{L}_{\rm FP}(t)$ implies Floquet-type solutions [10,11]:

$$P_\mu(x,v,t;\varphi)=e^{-\mu t}p_\mu(x,v,t;\varphi)\ , \tag{5}$$

where p_μ is a periodic function of the time, i.e., $p_\mu(x,v,t+\pi;\varphi)=p_\mu(x,v,t;\varphi)$. Inserting (5) into the Fokker-Planck equation yields the non-Hermitian eigenvalue problem, i.e.,

$$\left[\mathcal{L}_{\rm FP}-\frac{\partial}{\partial t}\right]p_\mu(x,v,t;\varphi)=-\mu p_\mu(x,v,t;\varphi)\ , \tag{6}$$

with generally complex-valued Floquet eigenvalues μ. The splitting of the Floquet solution into a product of a periodic function and an exponential is not unique; i.e., with $\tilde{p}_\mu(x,v,t;\varphi)=p_\mu(x,v,t;\varphi)e^{2ikt}$, we have

$$e^{-\mu t}p_\mu(x,v,t;\varphi)=e^{-(\mu+2ik)t}\tilde{p}_\mu(x,v,t;\varphi)\ , \tag{7}$$

where $k=0,\pm1,\pm2,\ldots$. Therefore the eigenvalues μ are defined modulo $2ik$. Further on, we choose the set of Floquet solutions with $\mathrm{Im}(\mu)\in[-1,1]$.

Within the stability zones of the deterministic parametric oscillator [see Eq. (14) below] it can be shown [11] that $P(x,v,t;\varphi)$ for large times approaches an asymptotic periodic probability density $P_{\rm as}(x,v,t;\varphi)$, being the Floquet-type solution for the vanishing Floquet eigenvalue $\mu=0$. Considering the intrinsic dynamical symmetry of the problem in (4) the asymptotic probability must be invariant under the parity symmetry transformation $\mathcal{T}:x\to-x,v\to-v$ [10,11]. This implies that $P_{\rm as}(x,v,t;\varphi)$ is symmetric at all times t, i.e., $P_{\rm as}(x,v,t;\varphi)=P_{\rm as}(-x,-v,t;\varphi)$. The bounded asymptotic long-time mean values defined by

$$\langle f(x,v,t;\varphi)\rangle_{\rm as}=\int P_{\rm as}(x,v,t;\varphi)f(x,v,t;\varphi)dx\,dv \tag{8}$$

are therefore periodic in time for all functions f that are invariant under $\mathcal{T}$, and identical zero for functions f that change sign with respect to the transformation $\mathcal{T}$.

A common experimental situation is that the phase φ is not controlled explicitly. Experimentally one usually averages over the phase by taking the average over experimentally obtained time series. With φ being uniformly distributed, this procedure becomes equivalent with an average over the phase [5]. Using this procedure, one measures the time-independent phase-averaged asymptotic probability and mean values, respectively, i.e.,

$$\bar{P}(x,v)=\frac{1}{2\pi}\int_0^{2\pi}P_{\rm as}(x,v,t;\varphi)d\varphi\ ,$$
$$\overline{\langle f(x,v)\rangle}=\frac{1}{2\pi}\int_0^{2\pi}\langle f(x,v,t;\varphi)\rangle_{\rm as}d\varphi\ .$$

In the following all overbars denote an average over the phase.

III. MEAN VALUES AND VARIANCES

A. Mean values

We first address the evaluation of the mean values of the state variables occurring in (4). From the Langevin equation (3) we see that the mean value $\langle x(t;\varphi)\rangle$ obeys the deterministic differential equation

$$\frac{d^2}{dt^2}\langle x\rangle+\gamma\frac{d}{dt}\langle x\rangle+[\omega_0^2+2\epsilon\cos(2t+\varphi)]\langle x\rangle=0\ . \tag{9}$$

With the substitution $\langle x\rangle=\langle y\rangle\exp(-\gamma t/2)$, one removes the damping contribution such that Eq. (9) can be cast into the standard form of a Mathieu equation of an undamped parametric oscillator [4], i.e.,

$$\frac{d^2}{dt^2}\langle y\rangle+\left[\omega_0^2-\frac{\gamma^2}{4}+2\epsilon\cos(2t+\varphi)\right]\langle y\rangle=0\ . \tag{10}$$

This equation cannot be solved in explicit form. From the Floquet theory for an ordinary second-order differential equation, we know that the two independent solutions of (10) are given by

$$f_1(t;\varphi)=e^{i\nu[t+(\varphi/2)]}p\left[t+\frac{\varphi}{2}\right]\ ,$$
$$f_2(t;\varphi)=f_1(-t;-\varphi)\ , \tag{11}$$

where $p(t)$ is a periodic function of time, i.e., $p(t+\pi)=p(t)$.

We see that the Floquet parameter ν governs the global behavior of the deterministic solution. In regions of the parameter space where ν is real, but not a whole number, both fundamental solutions are bounded. If ν becomes complex, one of the solutions grows exponentially. In the special case when ν is a whole number, one of the solutions is a periodic function with period π or 2π; the second independent solution is then found to be unstable [4].

In addition to an ambiguity in the definition of the Floquet parameter ν analogous to that addressed in (7), there exists a second one with regard to the sign of ν: Because of the structure of the solutions, we cannot decide whether ν or $-\nu$ is the true Floquet parameter. Therefore we introduce the following convention to determine the Floquet parameter unequivocally: If ν is a real number, we first select the set of Floquet solutions with $\mathrm{Re}(\nu)\in[-1,1]$. Through the additional freedom of choice between ν and $-\nu$ we can then always obtain a positive value of the Floquet parameter lying in [0,1]. In the case that ν is a purely imaginary number we select the ν value with a positive imaginary part. If ν is a complex number we select, as in the case above, a positive imaginary part. The real part is always an odd integer number, i.e., $\mathrm{Re}(\nu)=2k+1$ with $k=0,\pm1,\pm2,\ldots$ [see formula (12) below], and we subtract $2k$ to obtain $\mathrm{Re}(\nu)=1$.

To calculate the Floquet coefficient ν for (10), we use the formula [4]

$$\cos\pi\nu=\phi_2\left[t=\pi-\frac{\varphi}{2};\varphi\right], \tag{12}$$

where ϕ_1 and ϕ_2 are solutions of (10) with the initial values $\phi_1(0;\varphi)=0$, $\phi_2(0;\varphi)=1$, $\dot{\phi}_1(0;\varphi)=1$, and $\dot{\phi}_2(0;\varphi)=0$. ϕ_1 and ϕ_2 are calculated via a numerical integration of the differential equation (10). One distinguishes between three different cases:

$$\phi_2\left[\pi-\frac{\varphi}{2};\varphi\right]>1:\ \nu=\frac{i}{\pi}\operatorname{arcosh}\phi_2\left[\pi-\frac{\varphi}{2};\varphi\right]\Rightarrow\nu\text{ purely imaginary}, \tag{13a}$$

$$-1\le\phi_2\left[\pi-\frac{\varphi}{2};\varphi\right]\le 1:\ \nu=\frac{1}{\pi}\arccos\phi_2\left[\pi-\frac{\varphi}{2};\varphi\right]\Rightarrow\nu\text{ real}, \tag{13b}$$

$$-1>\phi_2\left[\pi-\frac{\varphi}{2};\varphi\right]:\ \nu=\frac{i}{\pi}\operatorname{arcosh}\left|\phi_2\left[\pi-\frac{\varphi}{2};\varphi\right]\right|+1\Rightarrow\nu\text{ complex valued}. \tag{13c}$$

Calculating ν for different points in the parameter space leads to the diagram in Fig. 1(a) that depicts the stable [white areas in Fig. 1(a)] and unstable regions (shaded areas) of the Mathieu equation (10). Changing the sign of ϵ is equivalent to a phase shift $\varphi\rightarrow\varphi'=\varphi+\pi$. This phase, however, has no influence on the stability of the solutions. The diagram is therefore symmetric to the $(\omega_0^2-\gamma^2/4)$ axis. In Fig. 1(a), the Floquet parameter ν equals 1 on the boundaries denoted by a_{2n+1} and b_{2n+1}. On the remaining boundaries ν equals zero.

The full solution of the damped parametric oscillator in (9) reads

$$\langle x(t;\varphi)\rangle=c_1e^{[i\nu-(\gamma/2)]t+i\nu(\varphi/2)}p\left[t+\frac{\varphi}{2}\right]+c_2e^{-[i\nu+(\gamma/2)]t-i\nu(\varphi/2)}p\left[-t-\frac{\varphi}{2}\right]. \tag{14}$$

Here c_1 and c_2 are determined through the initial values of $\langle x(t;\varphi)\rangle$ and $\langle\dot{x}(t;\varphi)\rangle$. We can—dependent on the parameter values—distinguish between three different kinds of asymptotic (i.e., $t\rightarrow\infty$) solutions. If ν is real or complex with $\mathrm{Im}(\nu)<\gamma/2$, then $\langle x(t;\varphi)\rangle_{\mathrm{as}}=0$. The mean $\langle x(t;\varphi)\rangle_{\mathrm{as}}$ oscillates with period π or 2π, if $\mathrm{Im}(\nu)=\gamma/2$. If $\mathrm{Im}(\nu)>\gamma/2$ the mean value $\langle x(t;\varphi)\rangle_{\mathrm{as}}$ grows exponentially. Figure 1(b) shows the stability diagram for $\gamma=0$ and 0.4. The solid lines form the stability diagram for zero friction, while the dotted lines give new stability zones at finite friction $\gamma=0.4$. The unstable regions are reduced to the shaded areas. The effect of damping results in two effects: (i) It increases the regions of bounded solutions; the zones of unbounded solutions no longer reach the ω_0^2 axis. (ii) The zones of stability are shifted through the damping to higher values of ω_0^2. This is especially visible for larger values of ϵ; it stems from the fact that we calculated ν for the shifted Mathieu equation (10) with $\omega_0^2\rightarrow\omega_0^2-\gamma^2/4$. The behavior of the lowest boundary line is different. Independent of the value of γ it always starts at $\omega_0^2=\epsilon=0$. With increasing friction γ the lowest stability zone reaches asymptotically the ϵ axis; in particular, for $\gamma\rightarrow\infty$ the solutions are always stable if $\omega_0^2\ge 0$, and unstable otherwise.

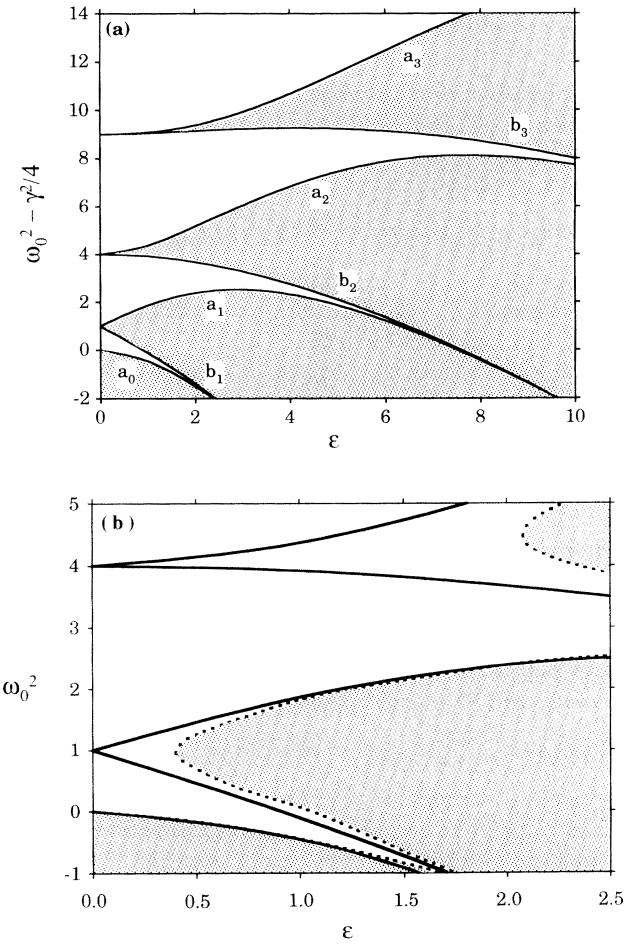

FIG. 1. (a) Stability chart for the Mathieu equation (10) with shifted angular frequency $\omega_0^2\rightarrow\omega_0^2-\gamma^2/4$. The shaded areas, being bounded by the lines a_n and b_n, denote the regions of unstable solutions. The diagram is symmetrical about the ordinate axis. (b) Stability diagram for the damped parametric oscillator, Eq. (9), for the values $\gamma=0$ and 0.4. The solid lines denote the boundaries for stability for $\gamma=0$. With finite friction, i.e., $\gamma=0.4$, the regions of bounded solutions become extended as characterized by the dotted lines. The shaded areas denote the corresponding regions of instability.

B. Covariance matrix

Next we study the covariance matrix $\underline{\sigma}$ of the Brownian dynamics in (4), i.e.,

$$\underline{\sigma}(t;\varphi)=\begin{bmatrix}\sigma_{xx}(t;\varphi) & \sigma_{xv}(t;\varphi)\\ \sigma_{vx}(t;\varphi) & \sigma_{vv}(t;\varphi)\end{bmatrix}$$
$$=\begin{bmatrix}\langle x^2\rangle-\langle x\rangle^2 & \langle xv\rangle-\langle x\rangle\langle v\rangle\\ \langle xv\rangle-\langle x\rangle\langle v\rangle & \langle v^2\rangle-\langle v\rangle^2\end{bmatrix}. \tag{15}$$

Because we are dealing with a linear problem, the conditional probability solution of (4) is of Gaussian form [12], i.e.,

$$P(x,v,t|x',v',0;\varphi)=\frac{1}{2\pi}\frac{1}{\sqrt{\det\underline{\sigma}}}\exp\left[-\frac{\sigma_{vv}}{2\det\underline{\sigma}}(x-\langle x\rangle)^2\right]$$
$$\times\exp\left[\frac{\sigma_{xv}}{\det\underline{\sigma}}(x-\langle x\rangle)(v-\langle v\rangle)-\frac{\sigma_{xx}}{2\det\underline{\sigma}}(v-\langle v\rangle)^2\right], \tag{16}$$

with the initial condition

$$P(x,v,0;\varphi)=\delta(x-x')\delta(v-v').$$

This initial condition implies that $\underline{\sigma}(0)=\underline{0}$.

Taking the phase φ explicitly into account, as a generalization of [7] for the Green's function we write

$$G(t,s;\varphi)=\phi_1(t;\varphi)\phi_2(s;\varphi)-\phi_1(s;\varphi)\phi_2(t;\varphi). \tag{17}$$

In terms of the Green's function, a formal solution of (1) with $x(t=0)=x(0)$ and $\dot{x}(0)$ reads

$$x(t;\varphi)=\sqrt{\gamma D}\int_0^t ds\,G(t,s;\varphi)\xi(s)e^{(\gamma/2)(s-t)}+\dot{x}(0)\phi_1(t;\varphi)e^{-(\gamma/2)t}+x(0)\left[\phi_2(t;\varphi)+\frac{\gamma}{2}\phi_1(t;\varphi)\right]e^{-(\gamma/2)t}. \tag{18}$$

This in turn yields for the elements of the covariance matrix:

$$\sigma_{xx}(t;\varphi)=2\gamma D\int_0^t ds\,G^2(t,s;\varphi)e^{\gamma(s-t)}, \tag{19a}$$

$$\sigma_{xv}(t;\varphi)=2\gamma D\int_0^t ds\left[G(t,s;\varphi)\frac{d}{dt}G(t,s;\varphi)-\tfrac{1}{2}\gamma G^2(t,s;\varphi)\right]e^{\gamma(s-t)}, \tag{19b}$$

$$\sigma_{vv}(t;\varphi)=2\gamma D\int_0^t ds\left\{\left[\frac{d}{dt}G(t,s;\varphi)\right]^2-\gamma G(t,s;\varphi)\frac{d}{dt}G(t,s;\varphi)+\tfrac{1}{4}\gamma^2G^2(t,s;\varphi)\right\}e^{\gamma(s-t)}. \tag{19c}$$

The covariance matrix remains bounded for parameter values that are located within the zones of stability for the damped deterministic equation (9). This can be seen if we take for $\phi_{1,2}$ linear combinations of the Floquet solutions $f_{1,2}$ in (11). Inspection of the exponential terms in (19) then shows that $\underline{\sigma}$ is bounded and asymptotically periodic if ν is real or $\mathrm{Im}(\nu)<\gamma/2$ [7]. If $\mathrm{Im}(\nu)=\gamma/2$ the covariance matrix diverges linearly in t, modulated by a periodic function. Within the zones of instability the covariance matrix elements consist of an exponentially growing function with a superimposed periodic modulation.

For our numerical calculations of $\underline{\sigma}$, it is advantageous to follow a different approach. With the relation [13]

$$\frac{d}{dt}\langle f(x(t),v(t))\rangle=\langle\mathcal{L}_{\mathrm{FP}}^{\dagger}f(x(t),v(t))\rangle, \tag{20}$$

we obtain a closed system of differential equations for the elements of the covariance matrix, i.e.,

$$\dot{\sigma}_{xx}=2\sigma_{xv}, \tag{21a}$$

$$\dot{\sigma}_{xv}=-\gamma\sigma_{xv}-[\omega_0^2+2\epsilon\cos(2t+\varphi)]\sigma_{xx}+\sigma_{vv}, \tag{21b}$$

$$\dot{\sigma}_{vv}=-2\gamma\sigma_{vv}-2[\omega_0^2+2\epsilon\cos(2t+\varphi)]\sigma_{xv}+2\gamma D. \tag{21c}$$

This system of coupled first-order ordinary differential equations has been solved numerically for different values of ϵ. The results are plotted in Figs. 2(a) and 2(b), respectively. As predicted from (8) we infer from Figs. 2 that the variance σ_{xx} oscillates with period π if $0<\epsilon<\epsilon_{\mathrm{cr}}$. Here, ϵ_{cr} is the value of the driving strength at which the motion becomes unbounded. For the chosen parameter values the critical ϵ value equals $\epsilon_{\mathrm{cr}}=1.05\ldots$. The amplitude of the variance increases if ϵ increases. For $\epsilon>\epsilon_{\mathrm{cr}}$, σ_{xx} grows exponentially in time. For reasons of comparison we depict all three covariance elements in Fig. 2(b).

Next we average over the uniformly distributed phase. The phase-averaged asymptotic long-time values of the

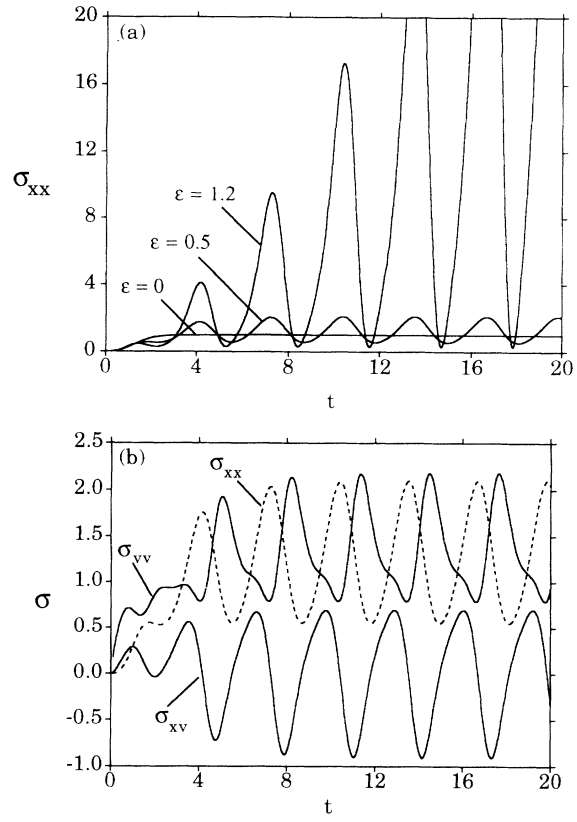

FIG. 2. (a) Variance σ_{xx} vs time t at $\gamma=1$, $D=1$, $\varphi=0$, and $\omega_0^2=1$ for varying driving strengths $\epsilon=0$, 0.5, and 1.2. (b) Plot of all three variances σ_{xx}, σ_{xv}, and σ_{vv} vs time t at $\gamma=1$, $D=1$, $\varphi=0$, $\omega_0^2=1$, and $\epsilon=0.5$.

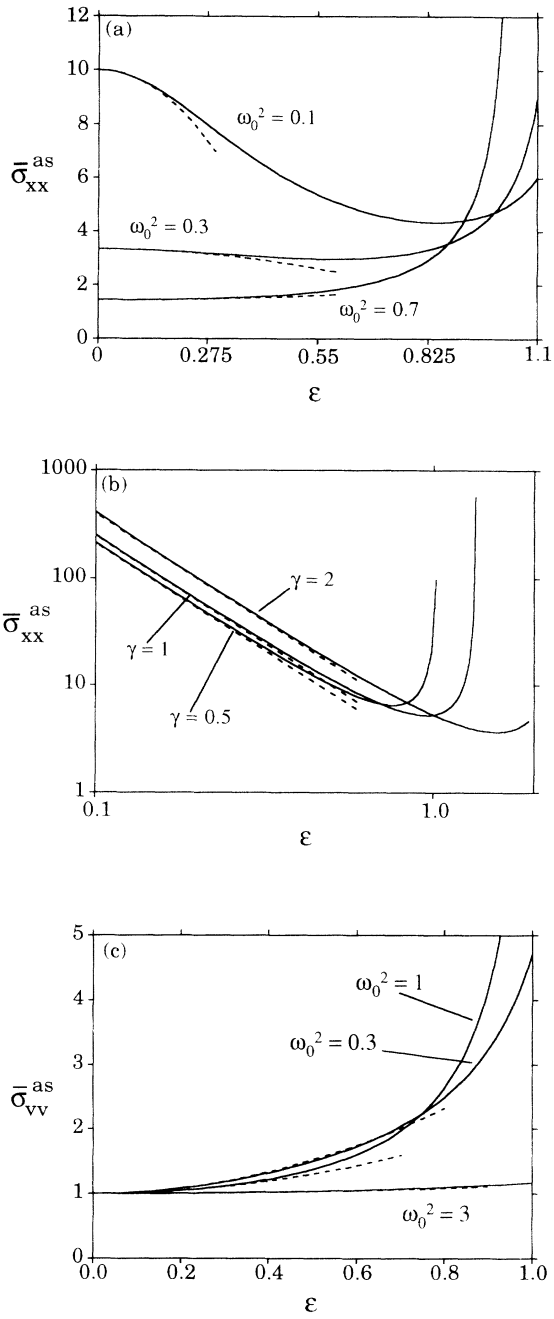

FIG. 3. (a) Phase-averaged coordinate variance $\bar{\sigma}_{xx}^{as}$ as a function of the modulation ϵ at $\gamma=1$ and $D=1$ for different values of the angular frequency $\omega_0^2=0.1$, 0.3, and 0.7. The numerically computed values are depicted by solid lines, while the dashed lines denote the analytic approximations for small modulation ϵ [cf. Eq. (26)]. (b) Phase-averaged coordinate variance $\bar{\sigma}_{xx}^{as}$ vs modulation ϵ for the case with $\omega_0^2=0$. $\bar{\sigma}_{xx}^{as}$ is plotted for $D=1$ and several values of the damping $\gamma=0.5$, 1, and 2. Again the numerically computed values are depicted by solid lines, while the dashed lines denote the analytic approximations for small modulation ϵ [cf. Eq. (29)]. (c) Phase-averaged velocity variance $\bar{\sigma}_{vv}^{as}$ as a function of the modulation ϵ at $\gamma=1$ and $D=1$ for varying angular frequency $\omega_0^2=0.3$, 1, and 3. As before, the numerically computed values are depicted by solid lines, while the dashed lines denote the analytic approximations for small modulation ϵ [cf. Eq. (30b)].

diagonal elements, i.e., $\bar{\sigma}_{xx}^{as}$ and $\bar{\sigma}_{vv}^{as}$, are depicted in Figs. 3. It can be noted from Fig. 3(a) that for positive-valued ω_0^2, being smaller than some threshold value [see (28) below], $\bar{\sigma}_{xx}^{as}$ first decreases with increasing ϵ, goes through a minimum, and then increases again. Above this threshold value, $\bar{\sigma}_{xx}^{as}$ increases monotonically. A similar minimum has been discovered experimentally for the first time in [8] for the case with $\omega_0^2=0$. This specific situation with $\omega_0^2=0$ is featured in Fig. 3(b), where $\bar{\sigma}_{xx}^{as}$ increases proportionally to ϵ^{-2} as $\epsilon\to 0$. Here the limit $\epsilon\to 0$ corresponds to a free particle for which $\sigma_{xx}^{as}(t)$ increases linearly with time.

In clear contrast to the behavior of the position variance, the corresponding phase (time)-averaged velocity variance increases monotonically with increasing ϵ, cf. Fig. 3(c). The behavior of $\bar{\sigma}_{xv}^{as}$ is not depicted because it equals zero for all values ω_0^2, $\epsilon<\epsilon_{cr}$.

In order to gain more insight into these results, we approximate σ_{xx} for small values of the modulation ϵ. Upon an elimination of σ_{xv} and σ_{vv} in (21), one finds for σ_{xx} a third-order differential equation, i.e.,

$$\dddot{\sigma}_{xx}+3\gamma\ddot{\sigma}_{xx}+\{4[\omega_0^2+2\epsilon\cos(2t+\varphi)]+2\gamma^2\}\dot{\sigma}_{xx}+\{4\gamma[\omega_0^2+2\epsilon\cos(2t+\varphi)]-8\epsilon\sin(2t+\varphi)\}\sigma_{xx}=4\gamma D. \tag{22}$$

We consider only parameter values that lead to a real Floquet coefficient ν or to $\mathrm{Im}(\nu)<\gamma/2$. Then σ_{xx} is periodic in the asymptotic regime $t\to\infty$. Setting in terms of a Fourier series

$$\sigma_{xx}^{\mathrm{as}}(t;\varphi)=\sum_{n=-\infty}^{\infty} a_n e^{in(2t+\varphi)} , \tag{23}$$

one obtains upon insertion of (23) into (22) the inhomogeneous tridiagonal recurrence relation

$$\epsilon A_n^- a_{n-1}+A_n a_n+\epsilon A_n^+ a_{n+1}=4\gamma D\delta_{n0} , \tag{24a}$$

where

$$A_n^-=4i(2n-1)+4\gamma , \tag{24b}$$

$$A_n=-8in^3-12\gamma n^2+(4\omega_0^2+2\gamma^2)2in+4\gamma\omega_0^2 , \tag{24c}$$

$$A_n^+=4i(2n+1)+4\gamma . \tag{24d}$$

This system of recurrence relations can be solved in terms of continued fractions [14]. Expanding the continued fraction in powers of ϵ yields up to order ϵ^2, with $\omega_0^2\neq 0$:

$$\sigma_{xx}^{\mathrm{as}}(t;\varphi)=\frac{D}{\omega_0^2}+\frac{D}{2\gamma\omega_0^4}\mathrm{Re}\left[\frac{A_0^- A_{-1}^+}{A_{-1}}\right]\epsilon^2-2\epsilon\frac{D}{\omega_0^2}\left[\mathrm{Re}\left[\frac{A_1^-}{A_1}\right]\cos(2t+\varphi)-\mathrm{Im}\left[\frac{A_1^-}{A_1}\right]\sin(2t+\varphi)\right]$$
$$+2\epsilon^2\frac{D}{\omega_0^2}\left[\mathrm{Re}\left[\frac{A_1^- A_2^-}{A_1 A_2}\right]\cos(4t+2\varphi)-\mathrm{Im}\left[\frac{A_1^- A_2^-}{A_1 A_2}\right]\sin(4t+2\varphi)\right] . \tag{25}$$

After averaging over the uniformly distributed phase, the asymptotic position variance equals

$$\bar{\sigma}_{xx}^{\mathrm{as}}=\frac{D}{\omega_0^2}+\frac{2D}{\omega_0^4}\frac{\gamma^2\omega_0^2-\gamma^2+3\omega_0^2-1}{(\omega_0^2\gamma-3\gamma)^2+(2-2\omega_0^2-\gamma^2)^2}\epsilon^2+O(\epsilon^4)$$
$$\equiv\frac{D}{\omega_0^2}+\Delta_{xx}\epsilon^2+O(\epsilon^4) . \tag{26}$$

We recall that the driving strength ϵ in (26) cannot be varied at will because it is restricted to belong to a zone of stability; note the stability diagram in Fig. 1(b).

For $\epsilon=0$ the variance takes on the value $\bar{\sigma}_{xx}^{\mathrm{as}}=D/\omega_0^2$, being in harmony with the equipartition theorem of the undriven harmonic oscillator. The parametric frequency yields a correction proportional to ϵ^2. Most importantly, we deduce from (26) that a minimum for $\bar{\sigma}_{xx}^{\mathrm{as}}$ emerges if Δ_{xx} become negative, i.e., if

$$\gamma^2\omega_0^2-\gamma^2+3\omega_0^2-1<0 . \tag{27}$$

The condition for the *existence of a minimum* for $\bar{\sigma}_{xx}^{\mathrm{as}}$ thus reads

$$0<\omega_0^2<\frac{1+\gamma^2}{3+\gamma^2} . \tag{28}$$

With ϵ small, we indeed find good agreement between the approximation in (26) and the numerical result [cf. Fig. 3(a)]. With $\gamma=1$ a minimum in $\bar{\sigma}_{xx}^{\mathrm{as}}$ exists for $\omega_0^2<0.5$.

Due to the divergence occurring in (26) for $\omega_0^2=0$, we study this limit separately. From the set of recurrence relations in (24) we find, for $\omega_0^2\to 0$ and $\epsilon\ll 1$,

$$\bar{\sigma}_{xx}^{\mathrm{as}}=\frac{D}{2}(4+\gamma^2)\frac{1}{\epsilon^2}+O(\epsilon^0) . \tag{29}$$

In clear contrast to the case with $\omega_0^2\neq 0$, the leading term is now proportional to ϵ^{-2}. Figure 3(b) displays the approximation in (29) together with the numerical results for different values of the damping coefficient γ.

In the foregoing discussion we studied $\bar{\sigma}_{xx}^{\mathrm{as}}$ by varying the driving amplitude ϵ, with all other parameters kept fixed. Next we study the dependence of the damping γ. From (26) we see that if ω_0^2 is within the range $\frac{1}{3}<\omega_0^2<1$, the variance $\bar{\sigma}_{xx}^{\mathrm{as}}$ is smaller than D/ω_0^2 for $\gamma^2>(1-3\omega_0^2)/(\omega_0^2-1)$. For $\gamma^2=(1-3\omega_0^2)/(\omega_0^2-1)$, $\bar{\sigma}_{xx}^{\mathrm{as}}$ assumes—up to order $O(\epsilon^4)$—the equilibrium value D/ω_0^2. Figure 4 shows the numerical result together with the approximation in (26). The extremal suppression below the equilibrium value occurs near $\gamma\approx 2.1$.

Next we turn to the remaining variance elements involving the velocity variable. Following the previous procedure, the phase-averaged long-time variances $\bar{\sigma}_{xv}^{\mathrm{as}}$ and $\bar{\sigma}_{vv}^{\mathrm{as}}$ follow from (21) and (25) as

$$\bar{\sigma}_{xv}^{\mathrm{as}}=0 , \tag{30a}$$

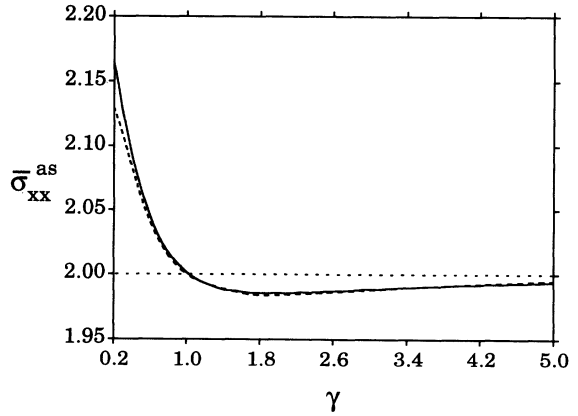

FIG. 4. Phase-averaged coordinate variance $\bar{\sigma}_{xx}^{\mathrm{as}}$ as a function of the damping γ at $\omega_0^2=0.5$, $D=1$, and $\epsilon=0.2$. The numerically computed value is depicted by a solid line. The dashed line denotes the analytic approximation for small modulation ϵ [cf. Eq. (26)]. The value for the variance at vanishing modulation ϵ, i.e., $\sigma_{xx}^{\mathrm{as}}=D/\omega_0^2$, is depicted by the dotted line.

$$\bar{\sigma}_{vv}^{\mathrm{as}} = D + \frac{2D}{\omega_0^2} \frac{1+\gamma^2+\omega_0^2}{(\omega_0^2\gamma - 3\gamma)^2 + (2-2\omega_0^2-\gamma^2)^2}\epsilon^2 + O(\epsilon^4)$$

$$\equiv D + \Delta_{vv}\epsilon^2 + O(\epsilon^4) \ . \tag{30b}$$

Setting $\epsilon=0$, we find the correct limiting results for the unperturbed oscillator, i.e., $\bar{\sigma}_{xv}^{\mathrm{as}}=0$ and $\bar{\sigma}_{vv}^{\mathrm{as}}=D$. The correction Δ_{vv} becomes negative for $\omega_0^2 < -1-\gamma^2$. In this regime, however, no periodic stable solutions exist for small ϵ, i.e., the ansatz (23) is then invalid. In agreement with our numerical findings we thus find that for $\omega_0^2>0$, $\bar{\sigma}_{vv}^{\mathrm{as}}$ does not exhibit a minimum, cf. Fig. 3(c).

However, we wish also to point out that for parameter values $\{\omega_0^2,\epsilon,\gamma\}$, corresponding to regions *between* zones of instability, the variances $\bar{\sigma}_{xx}^{\mathrm{as}}$ and $\bar{\sigma}_{vv}^{\mathrm{as}}$ trivially exhibit minima, and subsequently grow toward infinity as the boundaries of stability are reached.

The anomalous behavior of the averaged variance for the position coordinate deserves further discussion. For an unperturbed harmonic oscillator, equilibrium-statistical mechanics yields for the variances the well-known results given by the equipartition theorem, i.e., with $D=k_BT$,

$$\omega_0^2\langle x^2\rangle = D, \quad \langle v^2\rangle = D \ . \tag{31}$$

Our finding that, with $\omega_0^2\neq 0$, the variance for the position coordinate of a Brownian-damped parametric oscillator can be suppressed compared to the equilibrium value reveals future interesting physical and technical applications. With the parameters obeying the condition specified in (28), *the average mean-squared position fluctuations can be suppressed below the thermal limit* given in (31). Clearly, this fact does not imply a contradiction to statistical mechanics, because the parametrically driven oscillator represents an open statistical system for which the common laws of equilibrium thermodynamics are not applicable. It should be noted that the regime of parameter values guaranteeing this characteristic suppression are mainly located within the first stability zone [see Fig. 1(a)], and thus are readily experimentally accessible. For the situation with $\omega_0^2=0$, there occurs a similar characteristic initial drop of the variance, followed by a subsequent increase with increasing driving amplitude ϵ. This result has been confirmed experimentally very recently by Arnold, Folan, and Korn in Ref. [8], monitoring the parametric Brownian motion of a microsized polystyrene particle in a Paul trap. In agreement with (29) the experimental data for the time-averaged variance $\bar{\sigma}_{xx}^{\mathrm{as}}$ exhibit a characteristic decrease proportional to ϵ^{-2}, and after passing through a minimum the variance grows again as the driving strength ϵ approaches the boundary of stability. We remark that for $\omega_0^2=0$ and $\epsilon \ll 1$ the pseudopotential approximation used by Arnold, Folan, and Korn to describe the experiment yields the identical limiting result in (29).

It should be stressed that such a typical minimum for $\bar{\sigma}_{xx}^{\mathrm{as}}$ does not occur generically: For example, for the additively driven Brownian oscillator studied in [5], the phase-averaged asymptotic second mean increases monotonically with ϵ^2 [15].

IV. FLOQUET SPECTRUM

To determine the Floquet spectrum for a set of parameters which are located within the stability zones, we start with the eigenvalue problem (6), written in adjoint form

$$\left\{ v\frac{\partial}{\partial x} - \gamma v\frac{\partial}{\partial v} - x\left[\omega_0^2 + 2\epsilon\cos(2t+\varphi)\right]\frac{\partial}{\partial v} + \gamma D\frac{\partial^2}{\partial v^2} + \frac{\partial}{\partial t} \right\} p_{nm}^{\dagger} = -\mu_{nm}p_{nm}^{\dagger} \ , \tag{32}$$

where $n,m=0,1,2,\ldots$.

Because we deal with a two-dimensional nonseparable eigenvalue problem, we index the Floquet eigenvalue by two subscripts n and m. The adjoint eigenfunctions $p_{nm}^{\dagger}$ are periodic in t with period π, and consist of polynomials in x and v. For the calculation of the eigenvalue μ_{nm} it is sufficient to consider only the highest-order homogeneous polynomial m_{nm} being part of $p_{nm}^{\dagger}=m_{nm}+O(x^pv^q;p+q<N)$; i.e., with the order N given by $n+m=N$ we have

$$m_{nm} = a_1^{nm}(t)x^N + a_2^{nm}(t)x^{N-1}v + \cdots + a_{N-1}^{nm}(t)xv^{N-1} + a_N^{nm}(t)v^N \ . \tag{33}$$

Due to the linear structure, insertion of m_{nm} into (32), and comparison of equal powers of x and v yield a closed set of N coupled differential equations. The noise strength D does not enter into this system of equations because the diffusion operator maps a homogeneous polynomial of order N onto a homogeneous polynomial of order $N-2$. Hence the Floquet eigenvalues are independent of D. Put differently, it is therefore sufficient to infer the *spectrum* from a deterministic viewpoint. [The Floquet spectrum, as well as the corresponding adjoint Floquet functions, are determined in the Appendix by using the Fokker-Planck equation in (32) explicitly.] The solution of (1) in the absence of noise is given through Eq. (14) with $\langle x(t;\varphi)\rangle = x(t;\varphi)$. On the other hand, using for the probability the spectral decomposition

$$P(x,v,t;\varphi) = \sum c_{nm}e^{-\mu_{nm}t}p_{nm}(x,v,t;\varphi) \ , \tag{34}$$

we evaluate the Nth moment as

$$\langle x^N(t;\varphi)\rangle = x^N(t;\varphi) = \int P(x,v,t;\varphi)x^N dx\,dv = \sum_{n,m} b_{nm}^N(t;\varphi)e^{-\mu_{nm}t} \ , \tag{35}$$

where

$$b_{nm}^{N}(t;\varphi)=\int c_{nm}p_{nm}(x,v,t;\varphi)x^{N}dx\,dv\ . \tag{36}$$

If we equate (35) with (14), i.e.,

$$\left[c_1 e^{[i\nu-(\gamma/2)]t+i\nu(\varphi/2)}p\left[t+\frac{\varphi}{2}\right]+c_2 e^{-[i\nu+(\gamma/2)]t-i\nu(\varphi/2)}p\left[-t-\frac{\varphi}{2}\right]\right]^{N}=\sum_{n,m} b_{nm}^{N}(t;\varphi)e^{-\mu_{nm}t}\ , \tag{37}$$

we find upon a comparison of the time-dependent factors for different values of N the result for the Floquet spectrum, i.e.,

$$\mu_{nm}=n\mu_{10}+m\mu_{01},\quad n,m=0,1,2,\ldots, \tag{38a}$$

where

$$\mu_{10}=-i\nu+\frac{\gamma}{2},\quad \mu_{01}=i\nu+\frac{\gamma}{2}\ . \tag{38b}$$

In conclusion, the Floquet eigenvalues are given by a linear combination in terms of the basic stability coefficients μ_{10} and μ_{01} [see Eq. (14)]. This central result is similar to the behavior of the eigenvalues for a multidimensional Ornstein-Uhlenbeck process [16].

In Fig. 5 we depict the behavior of the Floquet eigenvalues μ_{10} and μ_{01} as a function of friction γ. The parameter ν is the Floquet coefficient of the deterministic parametric oscillator, cf. (10), with ω_0^2 substituted with $\omega_0^2-\gamma^2/4$. For zero friction, $i\nu$ is imaginary. Hence, $\mathrm{Re}(\mu)$ first grows proportionally to $\gamma/2$, cf. (38), while $\mathrm{Im}(\mu)$ is determined by ν, being dependent on ϵ and γ, cf. Fig. 1(a). The imaginary part of μ vanishes whenever ν reaches an upper boundary line a_{2n} in Fig. 1(a). Thus $i\nu$ becomes real valued, cf. Fig. 5(b), until—with increasing friction γ—a lower boundary line b_{2n} is hit. On the other hand, for parameter regions where ν is located between the lines a_{2n+1} and b_{2n+1}, we have $|\mathrm{Im}(\mu)|=1=|\mathrm{Re}(\nu)|$. With the friction increasing continuously, a bifurcation of μ takes place, yielding the bubblelike structure in Figs. 5(a) and 5(b). The number of bubbles occurring in $\mathrm{Re}(\mu)$ or $\mathrm{Im}(\mu)$, respectively, depends on the number of crossings of upper stability lines $a_n\to\cdots\to a_0<0$. If one initially starts with the $(n+1)$th zone of stability, and with the friction γ increasing from zero, the first bubble for $\mathrm{Re}(\mu)$ starts at $\gamma=2[\omega_0^2-a_n(\omega_0^2,\epsilon,\gamma)]^{1/2}$ and ends at $\gamma=2[\omega_0^2-b_n(\omega_0^2,\epsilon,\gamma)]^{1/2}$; this process is continued until one reaches the negative-valued zone boundary a_0. This is exemplified in Figs. 5, wherein with $\omega_0^2=5$ and $\epsilon=1$ one starts out at $\gamma=0$ from the $n=3$ zone of stability.

We also note the limiting behavior of the Floquet eigenvalues $\{\mu_{10},\mu_{01}\}$ when the friction γ assumes very large values, i.e.,

$$\mu_{10}=\frac{\omega_0^2}{\gamma}\quad\text{and}\quad\mu_{01}=\gamma-\frac{\omega_0^2}{\gamma}\quad\text{as}\ \gamma\to\infty\ . \tag{39}$$

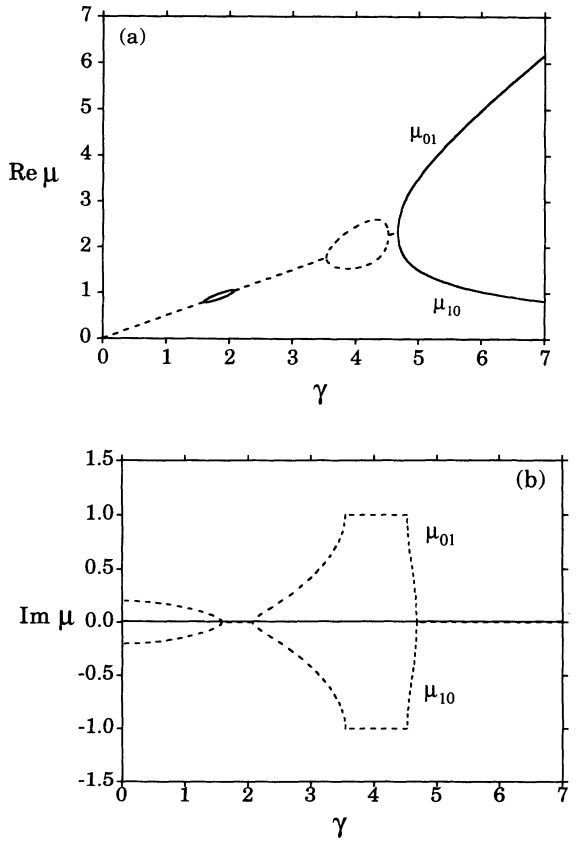

FIG. 5. The stability coefficients μ_{01} and μ_{10} are shown at $\omega_0^2=5$ and $\epsilon=1$ as a function of the damping γ. The real eigenvalues are plotted with solid lines in (a), whereas the real parts of the complex eigenvalues are depicted by dashed lines in (a). The imaginary parts are shown in (b).

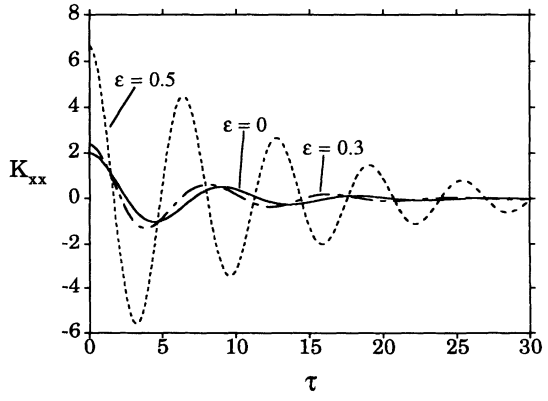

FIG. 6. Time-homogeneous autocorrelation function of the position variable, $K_{xx}(\tau)$, vs τ at $\omega_0^2=0.5$, $\gamma=0.3$, and $D=1$. The modulation ϵ takes on the values $\epsilon=0$, 0.3, and 0.5.

V. AUTOCORRELATION FUNCTION

In this last section we investigate the autocorrelation function K_{xx} of the position variable. The decay of this correlation is determined by the Floquet eigenvalues μ_{nm}, which enter the spectral representation of the autocorrelation [5,10,11]. Alternatively, the correlation can be expressed directly in terms of the solution of the Langevin equation in (1), i.e., in terms of the Green's function solution in (18) one finds

$$\begin{aligned} K_{xx}(t,t',\varphi) &= \langle x(t;\varphi)x(t';\varphi)\rangle \\ &= 2\gamma D e^{-(\gamma/2)(t+t')}\int_0^{t'} G(t,s;\varphi)G(t',s;\varphi)e^{\gamma s}ds \\ &\quad + [\dot{x}(0)\phi_1(t;\varphi)+x(0)\phi_2(t;\varphi)][\dot{x}(0)\phi_1(t';\varphi)+x(0)\phi_2(t';\varphi)]e^{-(\gamma/2)(t+t')} . \end{aligned} \tag{40}$$

This correlation is time inhomogeneous, due to the inherent nonstationarity of the Fokker-Planck process in (4). With phase φ being uniformly distributed, an average over the phase yields a time-homogeneous correlation [5,10,11] $K_{xx}(t,t',\varphi)\to K_{xx}(t-t'=\tau)$. The initial value $K_{xx}(\tau=0)$ coincides with $\bar{\sigma}_{xx}^{\rm as}$, whenever we consider parameter values (ϵ,γ) that lie within corresponding zones of stability; i.e., $\langle x(t\to\infty;\varphi)\rangle=\langle\dot{x}(t\to\infty;\varphi)\rangle=0$ in this case, cf. Sec. III A. The behavior of this phase-averaged time-homogeneous autocorrelation $K_{xx}(\tau)$ is depicted in Fig. 6 for three different sets of parameters. We remark that for parameter values $\{\omega_0^2,\epsilon,\gamma\}$ yielding a real-valued Floquet coefficient ν, the long-time decay of $K_{xx}(\tau)$ is governed solely by the friction γ, i.e.,

$$K_{xx}(\tau\to\infty)\propto\exp(-\gamma\tau/2),\quad \nu\text{:real} , \tag{41}$$

whereas the relaxation time is always enhanced whenever ν assumes complex values, i.e., with $\mathrm{Im}(\nu)<\gamma/2$ in the zones of stability one obtains

$$K_{xx}(\tau\to\infty)\propto\exp\{[\mathrm{Im}(\nu)-\gamma/2]\tau\},\quad \nu\text{:complex} . \tag{42}$$

Note that with $[\gamma/2-\mathrm{Im}(\nu)]<\gamma/2$, the corresponding bandwidth in the Fourier spectrum becomes *narrowed* as compared to the case in (41). We recall that this latter situation in (42) describes the dissipation-induced stabilization of an otherwise unstable behavior of the friction-free parametric oscillator.

The behavior of the velocity correlation K_{vv} and the cross correlation K_{xv} can be studied likewise. Again an average over the phase renders these correlations time homogeneous. Within the zones of stability the asymptotic mean values approach zero, i.e., all correlations $\{K_{xx}(\tau),K_{xv}(\tau),K_{vv}(\tau)\}$ approach zero as $\tau\to\infty$. Therefore, the spectral density $\bar{S}(\omega)=\int K(\tau)\exp(-i\omega\tau)d\tau$, does not—in clear contrast to the general behavior of systems exhibiting stochastic resonance [10,11]—exhibit δ-function contributions.

VI. CONCLUSIONS

In the present work we elucidated in detail the dynamics of noisy, dissipative parametric oscillators characterized by a time-periodic force constant. The statistical properties, such as the time-inhomogeneous (Gaussian) conditional probability, are solely determined by the behavior of the deterministic system (i.e., mean values) and the closed set of variance equations in (21). The time-averaged variances for the position and velocity variables exhibit an interesting behavior as a function of modulation strength ϵ and dissipation strength γ. Most importantly, we find the surprising result that the position variance can, within certain parameter regimes and $\omega_0^2\neq 0$, be suppressed below its corresponding thermal equilibrium value; note (26) and the discussion below (31). For the case with ω_0^2 set equal to zero, a similar characteristic bowl-shaped behavior with a minimum emerges for $\bar{\sigma}_{xx}^{\rm as}$ as well. This latter finding is in harmony with recent experimental results in Ref. [8]. The relaxation properties of general statistical quantities such as correlations, etc. are given in terms of the Floquet spectrum of the nonstationary Fokker-Planck equation in (4). We explicitly derived the whole Floquet spectrum $\{\mu_{nm}\}$ in Sec. IV. A second important finding is the atypical long-time relaxation behavior of the time-averaged position correlation discussed in Sec. V which shows a different relaxation time scale depending on whether the parametric oscillator is stable in absence or only in presence of friction γ [see Eqs. (41) and (42)]. These results (i.e., noise-induced parametric "squeezing") may prove useful for several applications in physics and engineering.

ACKNOWLEDGMENTS

We acknowledge financial support by Deutsche Forschungsgemeinschaft through Grant No. HA 1517/3-2, and by Stiftung Volkswagenwerk through Grant I/65-037-1.

APPENDIX

To obtain the first nonvanishing eigenvalues μ_{10} and μ_{01} and corresponding adjoint *Floquet functions* $p_{10}^{\dagger}$ and $p_{01}^{\dagger}$, respectively, we start with the ansatz

$$p_{10}^{\dagger}=a_1^{10}(t)x+a_2^{10}(t)v,\quad p_{01}^{\dagger}=a_1^{01}(t)x+a_2^{01}(t)v . \tag{A1}$$

Because of the invariance of the Fokker-Planck equation under the parity transformation defined in Sec. II, $p_{10}^{\dagger}$ and $p_{01}^{\dagger}$ must be odd [10,11]. Therefore they cannot obtain a term independent of x and v. Insertion of the ansatz into (32) and comparison of equal powers of x and v yields the equations (we suppress the indices of a_1 and a_2

for the moment)

$$-\omega_0^2 a_2-\epsilon\cos(2t+\varphi)a_2+\dot{a}_1=-\mu a_1\ ,$$
$$-\gamma a_2+a_1+\dot{a}_2=-\mu a_2\ . \tag{A2}$$

Eliminating a_1 leaves us with a second-order differential equation for a_2, i.e.,

$$\ddot{a}_2+(2\mu-\gamma)\dot{a}_2+[\omega_0^2+\mu(\mu-\gamma)+\epsilon\cos(2t+\varphi)]a_2=0\ . \tag{A3}$$

This again is a damped Mathieu equation. The function $a_2(t)$ must be determined so that a_2 is a periodic function. To this aim we make the transformation $a_2=\tilde{a}_2\exp[-(\mu-\gamma/2)t]$. This transformation does not only remove the damping term, but also removes the eigenvalue μ in the equation, i.e.,

$$\ddot{\tilde{a}}_2+\left[\omega_0^2-\frac{\gamma^2}{4}+\epsilon\cos(2t+\varphi)\right]\tilde{a}_2=0\ . \tag{A4}$$

Using for $\tilde{a}_2$ the Floquet solutions (11), we obtain for a_2 the two solutions

$$a_2^{01}=e^{i\nu[t+(\varphi/2)]}e^{-[\mu_{10}-(\gamma/2)]t}p\left[t+\frac{\varphi}{2}\right]\ ,$$
$$a_2^{10}=e^{i\nu[-t-(\varphi/2)]}e^{-[\mu_{01}-(\gamma/2)]t}p\left[-t-\frac{\varphi}{2}\right]\ . \tag{A5}$$

The periodicity condition for a_2 implies

$$i\nu-\mu_{01}+\frac{\gamma}{2}=0\ \text{ and }\ -i\nu-\mu_{10}+\frac{\gamma}{2}=0\ . \tag{A6}$$

Thus we obtain the first two Floquet eigenvalues:

$$\mu_{10}=-i\nu+\frac{\gamma}{2},\ \ \mu_{01}=i\nu+\frac{\gamma}{2}\ . \tag{A7}$$

Next (A5) can be inserted into (A2) to determine a_1^{01} and a_1^{10}. This yields explicitly the first (left) Floquet eigenfunctions $p_{01}^{\dagger}$ and $p_{10}^{\dagger}$.

For the higher-order Floquet eigenvalues μ_{02}, μ_{11}, and μ_{20}, we use the following ansatz for the adjoint Floquet functions $p_{02}^{\dagger}$, $p_{11}^{\dagger}$, and $p_{20}^{\dagger}$:

$$p_{02}^{\dagger}=a_0^{02}(t)+a_1^{02}(t)x^2+a_2^{02}(t)xv+a_3^{02}(t)v^2\ . \tag{A8}$$

$p_{11}^{\dagger}$ and $p_{20}^{\dagger}$ are defined analogically. The structure of these Floquet functions is determined by the fact that they must be even under the parity transformation mentioned above [10,11]. Again we insert this ansatz into (32). In doing so, for the coefficients a_1, a_2, and a_3 we obtain a closed system of three coupled differential equations. Upon an elimination of a_1 and a_2, one finds the corresponding equation of third order for a_3. The three independent solutions are given by

$$a_3^{20}=(\tilde{a}_2^{10})^2\exp[\tfrac{1}{2}(\gamma-\mu_{20})]\ ,$$
$$a_3^{11}=(\tilde{a}_2^{10}\tilde{a}_2^{01})\exp[\tfrac{1}{2}(\gamma-\mu_{11})]\ , \tag{A9}$$
$$a_3^{02}=(\tilde{a}_2^{01})^2\exp[\tfrac{1}{2}(\gamma-\mu_{02})]\ ,$$

with $\tilde{a}_2$ being a solution of (A4). The periodicity condition for a_3 determines the Floquet eigenvalues as

$$\mu_{20}=2\mu_{10},\ \ \mu_{11}=\mu_{10}+\mu_{01},\ \ \mu_{02}=2\mu_{01}\ . \tag{A10}$$

Knowing a_3 the coefficients a_0, a_1, and a_2 can be calculated. In principle it is possible to construct with this method all the other Floquet eigenvalues and *left eigenfunctions.*

[1] W. Paul, Rev. Mod. Phys. **62**, 531 (1990); W. Paul and M. Raether, Z. Phys. **140**, 262 (1955); E. Fischer, *ibid.* **156**, 1 (1959).

[2] P. Hänggi and C. Zerbe, in *Noise in Physical Systems and 1/f Fluctuations,* edited by P. H. Handel and A. L. Chung, AIP Conf. Proc. No. 285 (American Institute of Physics, New York, 1993), p. 481.

[3] E. Ott, C. Grebogi, and J. A. Yorke, Phys. Rev. Lett. **64**, 1196 (1990); **64**, 2837(E) (1990); A. Hübler, Helv. Phys. Acta **62**, 343 (1989); Z. Gills, C. Iwata, R. Roy, I. Schwartz, and I. Triandaf, Phys. Rev. Lett. **69**, 3169 (1992); Y. S. Kivshar, F. Rödelsperger, and H. Benner, Phys. Rev. E **49**, 319 (1994).

[4] N. W. McLachlan, *Theory and Application of Mathieu Functions* (Dover, New York, 1964); A. H. Nayfeh and D. T. Mook, *Nonlinear Oscillations* (Wiley, New York, 1979); W. Magnus and S. Winkler, *Hill's Equation* (Dover, New York, 1979).

[5] P. Jung and P. Hänggi, Phys. Rev. A **41**, 2977 (1990).

[6] M. Gitterman, R. J. Shrager, and G. H. Weiss, Phys. Lett. A **142**, 84 (1989).

[7] R. M. Mazo, J. Stat. Phys. **24**, 39 (1981).

[8] S. Arnold, L. M. Folan, and A. Korn, J. Appl. Phys. **74**, 4291 (1993).

[9] M. C. Wang and G. E. Uhlenbeck, Rev. Mod. Phys. **17**, 323 (1945).

[10] P. Jung and P. Hänggi, Europhys. Lett. **8**, 905 (1989); P. Hänggi, P. Jung, C. Zerbe, and F. Moss, J. Stat. Phys. **70**, 25 (1993).

[11] P. Jung, Phys. Rep. **234**, 175 (1993).

[12] P. Hänggi and H. Thomas, Phys. Rep. **88**, 207 (1982); see Sec. 1.3.E2 and Sec. 2.2.E2 therein.

[13] See Eq. (2.2.1b) in [12].

[14] H. Risken, *The Fokker-Planck Equation,* Springer Series in Synergetics Vol. 18 (Springer-Verlag, Berlin, 1984).

[15] For a dissipative oscillator with additive driving, the asymptotic mean values become periodic functions of time. The phase-averaged second mean $\overline{\langle x^2(t)\rangle}$ depends on the driving amplitude ϵ. Thus $\bar{\sigma}_{xx}^{\rm as}\equiv\overline{\langle x^2(t;\varphi)\rangle}-(\overline{\langle x(t;\varphi)\rangle})^2=\overline{\langle x^2(t;\varphi)\rangle}$, whereas $\bar{\sigma}_{xx}^{\rm as}=\overline{\langle x^2(t;\varphi)\rangle}-\overline{\langle x(t;\varphi)\rangle^2}=D/\omega_0^2$ becomes independent of external driving ϵ, and equals the unperturbed equilibrium value, cf. [5] and/or Eqs. (4.49) in [11].

[16] L. H'walisz, P. Jung, P. Talkner, L. Schimansky-Geier, and P. Hänggi, Z. Phys. B **77**, 471 (1989).

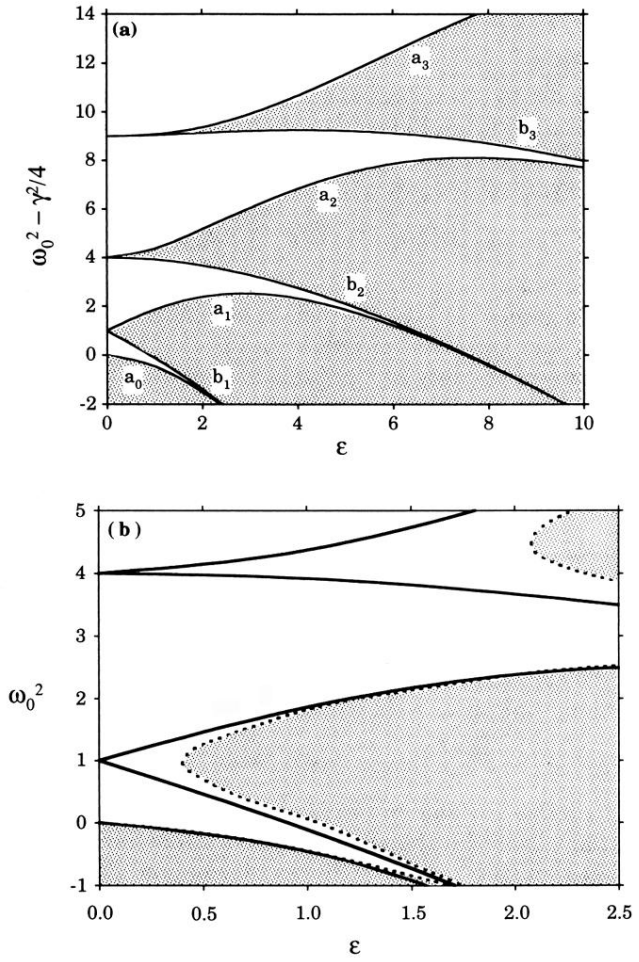

FIG. 1. (a) Stability chart for the Mathieu equation (10) with shifted angular frequency $\omega_0^2 \rightarrow \omega_0^2 - \gamma^2/4$. The shaded areas, being bounded by the lines a_n and b_n, denote the regions of unstable solutions. The diagram is symmetrical about the ordinate axis. (b) Stability diagram for the damped parametric oscillator, Eq. (9), for the values $\gamma = 0$ and 0.4. The solid lines denote the boundaries for stability for $\gamma = 0$. With finite friction, i.e., $\gamma = 0.4$, the regions of bounded solutions become extended as characterized by the dotted lines. The shaded areas denote the corresponding regions of instability.